A Novel Dispersion-Free Interleaver for Bidirectional DWDM Transmission Systems

Ming-Fang Huang, *Student Member, IEEE*, Jason (Jyehong) Chen, *Member, IEEE*, Jianjun Yu, *Senior Member, IEEE*, Sien Chi, *Fellow, OSA*, and Gee-Kung Chang, *Fellow, IEEE*, *Fellow, OSA*

***Abstract*—We propose a novel dispersion-free interleaver using optical delay lines by accurately locating the zeros in the transfer function. It has been implemented with the design of interleaver pairs with the same amplitude responses but opposite phase responses for bidirectional dense wavelength-division multiplexed (DWDM) transmission systems. The measured results are consistent with device simulation. We have further modified the original three-port design using unidirectional amplification, and a four-port interleaver has been built and demonstrated to achieve bidirectional DWDM transmission. In this paper, we fully studied and verified the applications of our four-port interleavers in bidirectional transmission. We demonstrated a bidirectional strain-line system over 210 km and a recirculating loop transmission over a 500-km standard single-mode fiber using 10-Gb/s ON–OFF keying signals. Furthermore, we also demonstrated return-to-zero differential phase-shift keying (DPSK) and nonreturn-to-zero DPSK modulation formats for more than 230 km of transmission. For comparison, the different amplification functions, such as the erbium-doped fiber amplifier and the semiconductor optical amplifier, have also been probed in this paper. The experimental results have clearly illustrated the desirable functions of this novel bidirectional amplifier in this dispersion-free interleaver.**

***Index Terms*—Birefringence, differential phase-shift keying (DPSK) modulation, interleaver, optical fiber communication, optical filters, wavelength-division multiplexed (WDM) optical fiber devices.**

I. Introduction

AS AN OPTICAL filter, an interleaver combines or separates a comb of dense wavelength-division multiplexed (DWDM) signals [1]–[3]. The periodic nature of the interleaver filter reduces the number of Fourier components that are required for a flat passband and a high-isolation rejection band. This behavior is in great contrast to the single-channel add/drop filters that synthesize a single narrow-band filter over a wide rejection band. Because the interleaver requires fewer Fourier components than a single narrow-band filter, the same flat-top sharp edge response of a higher order narrow-band filter can be realized using a small number of sections [1]. The filter function of an interleaver and its period can be separated. Interleavers have been shown to resolve a comb of DWDM frequencies with channel spacings of 100, 50, 25, and 12.5 GHz. The period of the interleaver is governed by the free-spectral range of the core elements, in which a longer optical path achieves a narrower channel spacing [2].

Although the interleaver has been widely used in multiplexing and demultiplexing of DWDM optical signals, its applications in bidirectional transmissions have not been fully studied and verified. With rapid growth of Internet traffic, it is desirable to increase the capacity of DWDM optical networks by using spectral efficiency and high-bit-rate transmissions [4]. Bidirectional transmission provides an effective method for DWDM networks to increase bandwidth utilization and reduce operating costs at the same time [5]–[7]. One of the core technologies in bidirectional transmission is bidirectional amplification, which requires high gain, low noise, and removing or reducing Rayleigh backscattering (RB) [8]. Currently, two key bidirectional transmission amplifier schemes have been demonstrated. One scheme is to use two circulators along with two regular erbium-doped fiber amplifiers (EDFAs), and the other scheme is to use semiconductor optical amplifiers (SOAs). The first scheme needs more optical components and more EDFAs; therefore, this scheme is not a cost-effective solution. The gains of EDFAs are typically limited to avoid the RB self-oscillation; these limitations will significantly shorten the amplification span and reduce the optical signal-to-noise ratio (OSNR) [9], thus increasing the operational cost and degrading the transmission quality. The main problems of the second scheme are the small gain and large crosstalk caused by cross-gain modulation (XGM) in SOA when the transmission signals have an ON–OFF keying (OOK) modulation format [5], [10]. A four-port interleaver has been proposed before [6] using fiber-based configuration. The device is sensitive to temperature variation and exhibits Gaussian passband characteristics. This paper proposed and experimentally demonstrated a new four-port interleaver with a temperature-compensated flat-top passband for dispersion-free transmission. The primary functions of the four-port interleaver are to redirect east and west traffic to an individual unidirectional transmission path in the interleaver while achieving simultaneous crosstalk and noise reduction.

Manuscript received January 12, 2007; revised July 16, 2007.

M.-F. Huang is with School of Electrical and Computer Engineering, Georgia Institute of Technology, Atlanta, GA 30332 USA, and also with the Institute of Electro-Optical Engineering and Department of Photonics, National Chiao Tung University, Hsinchu 300, Taiwan, R.O.C. (e-mail: mhuang9@ece.gatech.edu).

J. Chen is with the Institute of Electro-Optical Engineering and Department of Photonics, National Chiao Tung University, Hsinchu 300, Taiwan, R.O.C. (e-mail: jchen@mail.nctu.edu.tw).

J. Yu is with NEC Laboratories America, Princeton, NJ 08540 USA (e-mail: jianjun@ece.gatech.edu).

S. Chi is with the Institute of Electro-Optical Engineering and Department of Photonics, National Chiao Tung University, Hsinchu 300, Taiwan, R.O.C., and also with the Department of Electrical Engineering, Yuan Ze University, Chungli 320, Taiwan, R.O.C. (e-mail: schi@mail.nctu.edu.tw).

G.-K. Chang is with the School of Electrical and Computer Engineering, Georgia Institute of Technology, Atlanta, GA 30332 USA (e-mail: gkchang@ece.gatech.edu).

Color versions of one or more of the figures in this paper are available online at http://ieeexplore.ieee.org.

Digital Object Identifier 10.1109/JLT.2007.907791

Among several choices of modulation and demodulation formats, special attention has been given to differential phase-shift keying (DPSK), which was proving to be superior [11] relative to the traditional OOK in an optical fiber communication system. This is due to its larger tolerance to fiber nonlinearity and noise from amplified spontaneous emission (ASE) [11]. Well-conducted experiments have indicated that bidirectional DPSK transmission attains optimal performance by using SOAs as inline amplifiers [10], [12]. However, in WDM systems, SOA needs to be operated above the saturation level to obtain the required OSNR at the receiver. However, the waveform distortion and XGM pose severe challenges to operate SOAs in the saturation region [12]–[14]. Due to the tolerance of DPSK modulation to various nonlinear effects such as self-phase modulation and cross-phase modulation, it has attracted much attention from researchers around the world. The experimental results show that optical signals using a DPSK modulation format can achieve ultralong-haul transmission [13], [15]. Most of the recent DPSK experiments used return-to-zero (RZ) signals rather than nonreturn-to-zero (NRZ) signals to achieve an optimal bandwidth/distance performance because the RZ shape can tolerate high input power and has a small intersymbol interference.

This paper is organized into five sections. Section II presents the design and implementation of the interleaver. Section III presents characterization and analysis regarding passband, insertion loss, temperature sensitivity, and dispersion characteristics of the interleaver. Experimental setup and demonstration of a bidirectional DWDM transmission system based on a four-port interleaver are presented in Section IV. Finally, the conclusions are summarized in Section V.

II. Considerations of an Interleaver Design

A birefringent crystal has long been used in designing optical filters, including birefringent crystal plates and polarizers. The two major types of birefringent filters are Lyot–Öhman filters and Šolc filters [16]–[18]. Both types are based on interference between polarized light and require phase retardation among the components of light polarized parallel to the slow and fast axes of the crystal as light passes through it. Consequently, the birefringent crystal is served as an optical delay line, and a half-wave plate is used to alter the polarization between the delay stages. The rotation of the half-wave plates can also be considered to be designed to generate various required Fourier frequency components.

Fig. 1 shows the configuration of the three-port interleaver employed by the birefringent crystal. At the input and outputs of the interleaver, a YVO_4 walk-off crystal and a half-wave plate were used to ensure that the optical delay cells contained only a single polarization. Each delay cell includes two birefringent crystals, namely YVO_4 and rutile (TiO_2), to compensate for the temperature variation. The lengths of YVO_4 and rutile can be determined using

$$\Delta n_1 L_1 - \Delta n_2 L_2 = m\lambda_{\text{center}} = \frac{c}{\text{FSR}} \tag{1}$$

$$\frac{d}{dT}(\Delta n_1 L_1 - \Delta n_2 L_2) = 0 \Rightarrow \Delta n_1 L_1 \beta_1 - \Delta n_2 L_2 \beta_2 = 0 \tag{2}$$

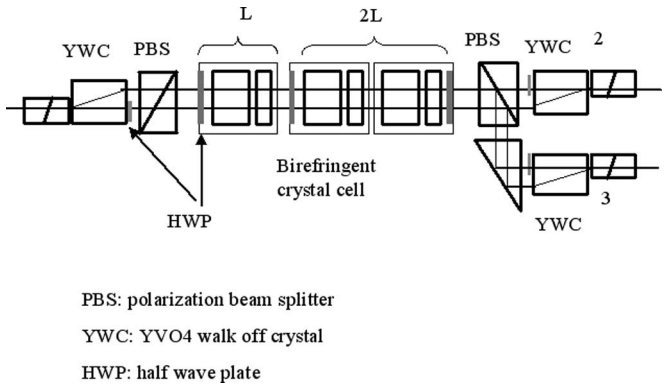

Fig. 1. Possible configuration of a three-port L–2L interleaver.

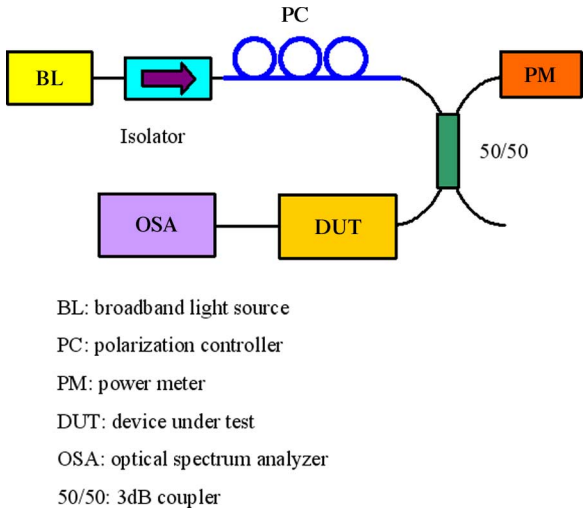

Fig. 2. Measurement setup of the birefringent crystal temperature sensitivity.

with

$$\beta_i \equiv \frac{d\Delta n_i}{\Delta n_i dT} + \frac{dL_i}{L_i dT} = \frac{d\lambda_i}{\lambda_i dT}, \qquad i = 1, 2.$$

In (1) and (2), Δn_1 and Δn_2 indicate the group index difference between ordinary and extraordinary axes of YVO_4 and rutile, respectively. Moreover, c denotes the speed of light, FSR represents the free spectral range, L_i represents the length of the crystal, λ_{center} denotes the center wavelength of the operation wavelength range, m represents the order of the birefringent wave plate, and β_i is the normalized variation in the wavelength with temperature. Fig. 2 shows the measurement setup that is used to determine β. For normal incident light, each crystal forms a Fabry–Pérot etalon cavity from the facets' reflection, and the transmission spectra will have null points with FSR determined by the cavity length. When we change the temperature of the crystal, the cavity length will change, and the null points will start to drift accordingly. β can then be determined by measuring the drifting of the null point with temperature in the optical spectrum analyzer (OSA). For YVO_4 and rutile, the group index differences are 0.2139 and 0.2652, and the β values are -26.54×10^{-6} $1/^{\circ}$C and -99.06×10^{-6} $1/^{\circ}$C, respectively. At the central frequency of 193.5 THz, the values of β correspond to 5.13 and 19.17 GHz/°C, respectively. For

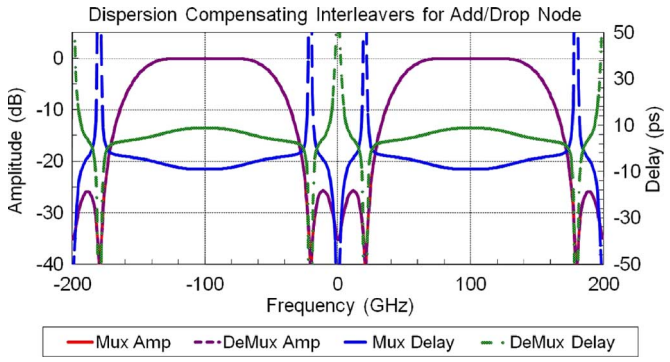

Fig. 3. Two types of interleavers with the same amplitude but opposite delay response.

a 100-GHz interleaver, FSR equals to 200 GHz, and solving (1) and (2) yields the lengths of the YVO_4 and rutile crystals, which are 9.5697 and 2.0685 mm, respectively [19]. After temperature compensation, the temperature drift is reduced to approximately 0.056 GHz/°C. This corresponds to about 3.7-GHz drift in temperature variation from 0 °C to 65 °C.

One difficulty that could not be fully compensated for during the design process was the wavelength dependence of refractive index, namely dispersion. However, as shown in Appendix, with a proper selection of crystal lengths, for a typical C-band application (with a center frequency of 193.5 THz and a total bandwidth 4 THz), the refractive index dispersion introduces a center frequency offset of only 2–2.5 GHz.

The optimized wave-plate angles were determined using the "minimize the integral square error" method, as shown in

$$\min\left\{\sum_{n=1}^{N}\left[\hat{x}(f_n)-x(f_n)\right]^2\right\} \tag{3}$$

with

$$f_c-\frac{\text{FSR}}{2}\le f_n\le f_c+\frac{\text{FSR}}{2}. \tag{4}$$

In (3), $\hat{x}(f_n)$ is the desired target amplitude response, and $x(f_n)$ is the real transmission function. The transmission function is periodic; therefore, the errors can be summed over one FSR at the central frequency f_c. By charging the position of the half-wave plate at the input walk-off crystal, the input polarization angle was shifted 90° and generates two delay responses. Minimizing (3) can yield the corresponding wave-plate angles. Fig. 3 presents the simulated amplitude and delay response of two types of interleavers. This figure shows that changing the input polarization yields two interleavers with the same amplitude responses but opposite delay responses. Therefore, the cascaded interleaver pair will have a constant delay, and therefore, the dispersion will approach zero.

To design an interleaver with a sharp edge response, higher Fourier frequency components must be included. Additional delay line stages are required to increase the highest Fourier frequency, and the passband, insertion loss, size, reliability, and cost are all traded off against one another. For a 100-GHz interleaver, L–2L–2L can meet the passband and delay requirements for 40-Gb/s transmission without difficulty. If only a 10-Gb/s signal is transmitted, an L–2L design will suffice.

III. Experimental Results of 100-GHz L–2L–2L Interleavers

After the design analysis, an L–2L–2L interleaver was fabricated to verify the design. Fig. 4(a) and (b) shows the measurement results of the recentered transmission responses in a frequency range from 191.8 to 195.5 THz at 0 °C, 23 °C, and 65 °C, respectively. The figures clearly demonstrate successful mitigation of the temperature variation. Fig. 4(c) shows the 0.5-dB passband of different channels at 0 °C, 23 °C, and 65 °C. The average 0.5-dB passband is about 73 GHz. Fig. 4(d) shows the polarization-dependent loss (PDL) of different channels at 0 °C, 23 °C, and 65 °C. The average PDL is below 0.15 dB, which means that there is a good control of the alignment between the input fiber and the walk-off YVO_4 crystal. The fiber alignment is similar to typical microoptic fiber devices such as isolator, circulator, and switch. The alignment needs to be very carefully done, and an active alignment is needed.

Fig. 5 plots the measured amplitude and delay responses of two types of 100-GHz interleavers. Fig. 5(a)–(d) illustrates type-A and type-B interleavers that have identical transmission spectra but reversed delay responses. Meanwhile, type-A and type-B interleavers can be cascaded to generate a linear-phase interleaver pair with a total dispersion near zero, which is a feature that is desirable, particularly in metro add/drop applications and/or high-bit-rate transmission systems. Fig. 6 plots the measured results that relate to seven cascaded interleaver pairs. The figure shows that the total delay is below 1 ps within the passband. Figs. 5 and 6 clearly show that interleavers with the same amplitude response and opposite delay response were successfully designed.

IV. Novel Bidirectional Transmission System Using Four-Port Interleavers

Through minor modification of the original three-port design, a novel four-port interleaver that enables bidirectional transmission using unidirectional amplification was demonstrated. The interleaver used in this paper is a symmetrical four-port interleaver with two input and two output ports. Fig. 7 shows the detailed configuration of the interleaver. Fig. 8(a) illustrates the measured amplitude response of the interleaver for even and odd channels. The channel spacing of this interleaver was 50 GHz, with an insertion loss of 2.2 dB and a 0.5-dB passband of approximately 35 GHz. The interleaver was designed to have complementary wavelength-dependent routing characteristics. For example, if λ_1 (odd channel) enters port 1, it is routed to port 4. However, when λ_2 (even channel) goes into port 2, it is also directed to port 4. By using this interleaver property, when east-even channels arrive at port 2 of the interleaver, they are sent to port 4. On the other hand, when the west-odd channels enter port 1 of the interleaver, they are also routed to port 4. Therefore, bidirectional transmission is routed into unidirectional transmission, and unidirectional amplification is achieved using a single EDFA, as shown in Fig. 8(b).

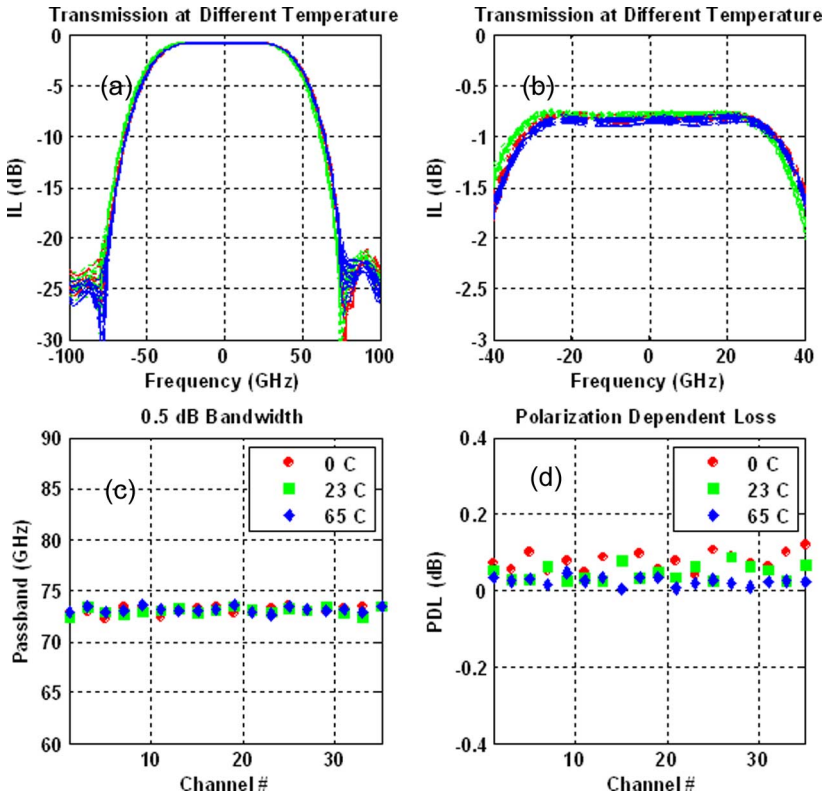

Fig. 4. (a) Recentered transmission at 0 °C, 23 °C, and 65 °C. (b) Magnified folded transmission at 0 °C, 23 °C, and 65 °C. (c) Passband of 0.5 dB at 0 °C, 23 °C, and 65 °C. (d) PDL at 0 °C, 23 °C, and 65 °C.

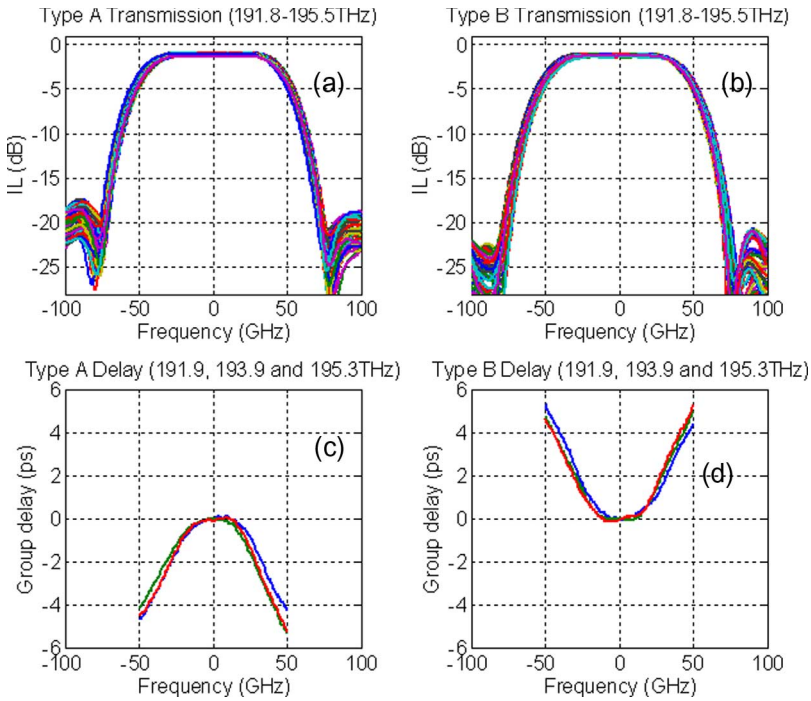

Fig. 5. (a) and (b) Measured recentered amplitude of the multiplexer (Mux) and demultiplexer (DeMux). (c) and (d) Measured folded delay of the Mux and DeMux.

A. Strain-Line Bidirectional Transmission System

To demonstrate this novel wavelength-sensitive routing characteristic of the four-port interleaver, a bidirectional transmission system was used, as illustrated in Fig. 9 [7]. A dual-stage EDFA with midstage dispersion compensation was employed to provide the unidirectional loss and dispersion compensation. The eight-channel laser sources consist of two groups: one from 1550.52 to 1551.72 nm and the other from 1554.54 to 1555.75 nm, all on the standard International Telecommunications Union (ITU) 50-GHz channel spacing grids. These eight

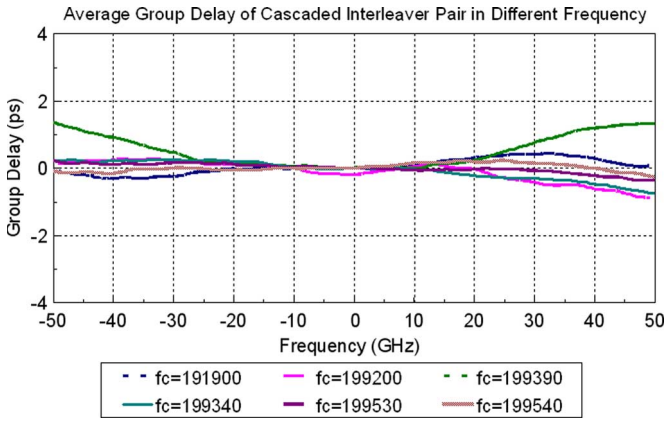

Fig. 6. Measured cascaded delay response for different frequencies.

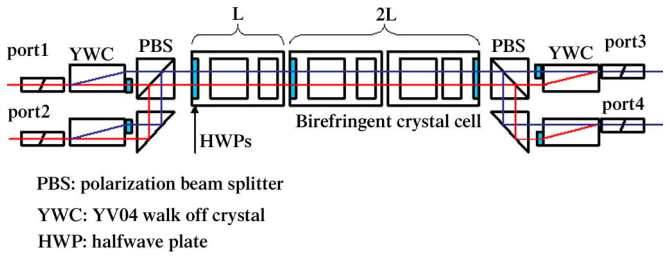

Fig. 7. Possible configuration of a four-port L–2L interleaver.

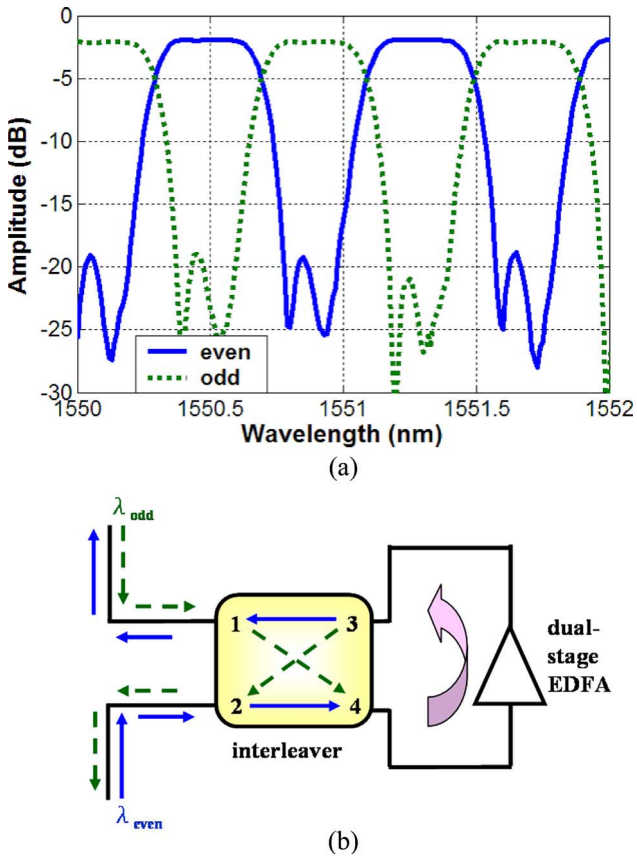

Fig. 8. (a) Transmission spectrum of a four-port interleaver. (b) Illustration of the working principle of a four-port interleaver.

lasers were separated into two parts, i.e., as even and odd channels for eastbound and westbound demonstrations. Both eastbound and westbound signals were individually modulated using a $LiNbO_3$ electrooptical modulator at 10 Gb/s with a pseudorandom binary sequence (PRBS) length of $2^{31}-1$ pattern. We used two 105-km standard single-mode fiber (SSMF) spoons for transmission. The total distance for the bidirectional transmission was 210 km. Within the dual-stage EDFA, a dispersion-compensating fiber (DCF) was inserted to compensate for the accumulated chromatic dispersion in 210 km of SSMF. The gains and noise figures (NFs) of the dual-stage EDFA at all channels were about 23.5 and 4.5 dB, respectively. Fig. 10(a) illustrates the bit-error-rate (BER) curves and the corresponding eye diagrams of the worst channel, namely channel 6. After 210 km of transmission, both the eye diagrams and BER curves indicate similar performance degradation due to the accumulated ASE noise and dispersion in the bidirectional and unidirectional transmission systems. Fig. 10(b) depicts the BER penalty of all channels. This figure clearly shows that the BER penalty variations between the bidirectional and unidirectional transmissions are less than 0.2 dB for all channels. When compared with the back-to-back BER curve, the sensitivity penalties are less than 0.8 dB for both cases. The inset figure within Fig. 10(b) is the received optical spectrum of the east-even channels ($\lambda = 1550.92,\ 1551.72,\ 1554.94,$ and 1555.74 nm) after 210 km of transmission. Because all the signals are rerouted from the bidirectional transmission into the unidirectional transmission at the amplification stage using an interleaver, the noise is considerably diminished. Consequently, the optical signals experience a much lower NF, as compared with an NF, exceeding 6.5 dB by using a linear optical amplifier [5]. Therefore, OSNRs exceeding 35 dB after 210 km of transmission at all channels were achieved by the proposed method, as compared with less than 26 dB of OSNR in [5].

B. Long-Distance Transmission Using a Bidirectional Recirculating Loop

To simulate long-distance transmission, a recirculating loop had been set up, as shown in Fig. 11 [20]. An interleaver was placed at the input of the recirculating loop to split the east and west channels for bidirectional transmission, and traffic directed the opposite way was combined for unidirectional amplification. Two spools of a 50-km Corning LEAF fiber were adopted in the recirculating loop. A dual-stage EDFA with a 5-km Corning DCF was employed in the midstage of the loop to compensate for the transmission loss and the accumulated dispersion in the LEAF fiber. The two interleavers in the loop were particularly arranged to reduce chromatic dispersion caused by the flat-top transmission band design of the interleaver [21]. Fig. 12(a) shows the receiving power penalties of all channels at a BER of 10^{-9} and the optical spectrum after 500 km. All channels had power penalties of less than 2.5 dB, and the penalty differential between them was less than 0.4 dB. The optical spectrum displays an OSNR of over 31 dB for all channels with a 0.02-nm resolution bandwidth on the OSA. Fig. 12(b) plots the BER curves and

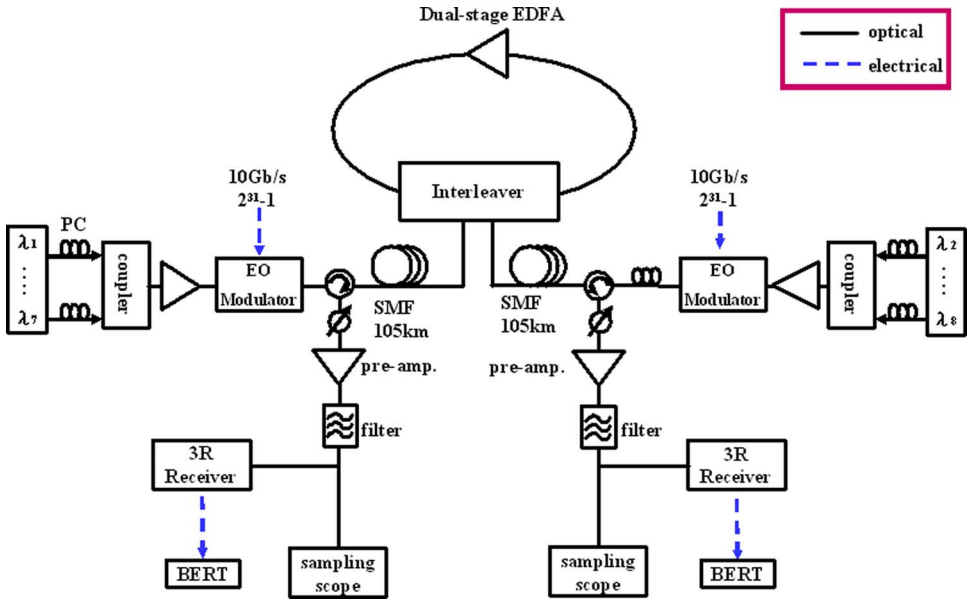

Fig. 9. Experimental setup of a strain-line bidirectional transmission system.

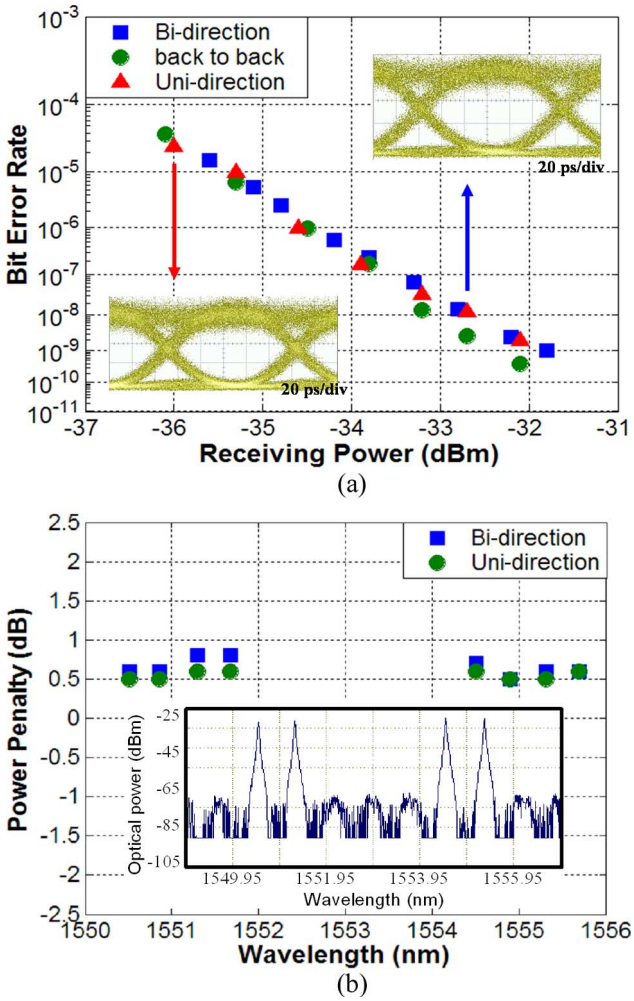

Fig. 10. (a) Worst channel BER curves and corresponding eye diagrams of the unidirectional and bidirectional transmissions. (b) Power penalty of the bidirectional and unidirectional transmissions and received optical spectrum for east-even channels after 210 km of bidirectional transmission.

the corresponding eye diagrams at channel 7 (back-to-back) for 100-, 300-, and 500-km transmission distances. The measured power penalties were about 0.3, 1, and 2 dB for 100-, 300-, and 500-km transmission distances, respectively, at a BER of 10^{-9} under optimal polarization conditions. The polarization controller was used to minimize the polarization effects such as the polarization-dependent gain and PDL in the recirculating loop. The penalties were attributed to ASE accumulation due to signal-to-noise ratio (SNR) degradation, resulting from the high link loss between the amplifier span.

C. Comparison Between Bidirectional DPSK and OOK Signals

The experimental setup for bidirectional DPSK transmission is shown in Fig. 13. Eight distributed-feedback lasers producing continuous-wave lightwaves, which were equally spaced by 50 GHz from 1556.56 to 1559.39 nm, all on the standard ITU grid, were combined and simultaneously modulated by a phase modulator (PM). The PM was driven by 10-Gb/s electrical data with a PRBS sequence length of $2^{31}-1$ to generate DPSK signals. The transmission fiber was a 230-km SSMF with a 3-dBm total launched power into each 115-km SSMF. The matched DCFs were adopted in the configuration to compensate for the accumulated dispersion in the SSMF. A dual-stage EDFA with a 24.5-dB gain was employed as the inline amplifier to compensate for the transmission loss. Fig. 14(a) shows the BER curves and the corresponding eye diagrams for three of the eight RZ-DPSK signals, namely channel 1 ($\lambda = 1556.55$ nm), channel 4 ($\lambda = 1557.77$ nm), and channel 8 ($\lambda = 1559.39$ nm). We can see that the penalty at a BER of 10^{-9} for channel 8 was less than 1.1 dB, and the clear eye indicates the good quality of the signals after a 230-km fiber. Fig. 14(b) compares the RZ-DPSK and NRZ-DPSK modulation performances after 230 km of transmission at channel 4. The RZ-DPSK signals

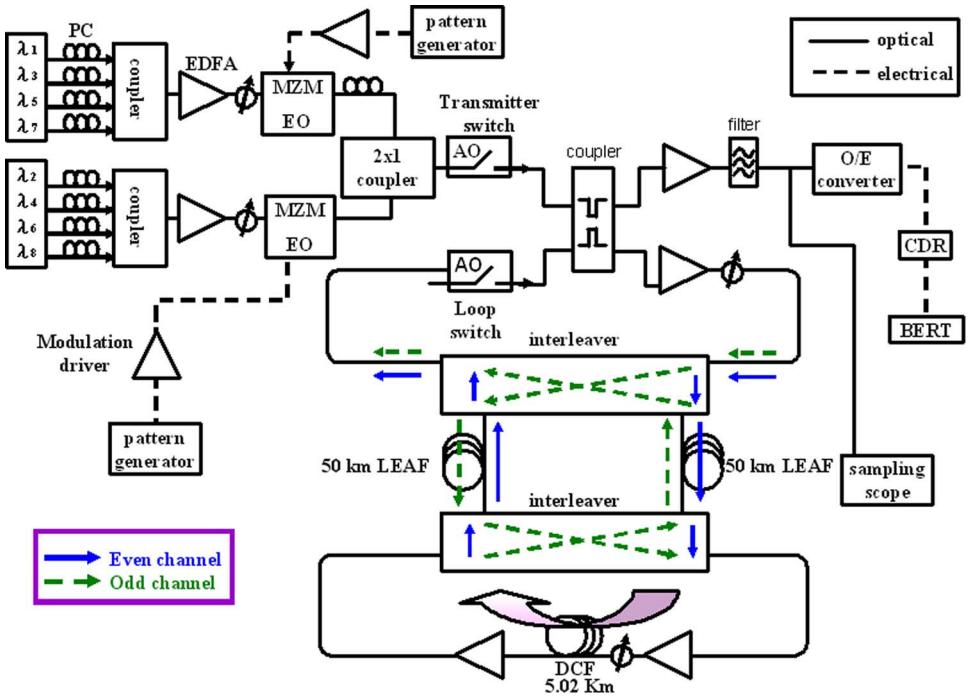

Fig. 11. Recirculating loop setup for a long-distance bidirectional transmission experiment.

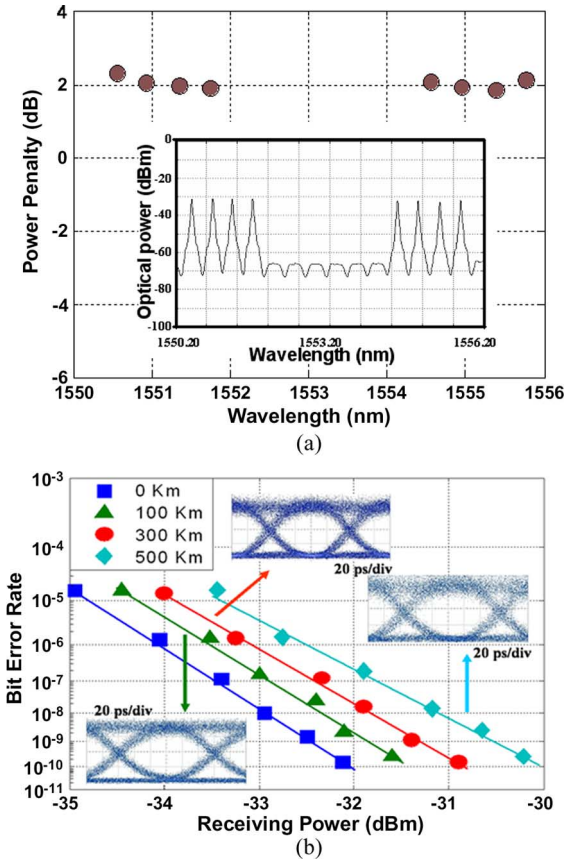

Fig. 12. (a) Received power penalties of all channels at a BER of 10^{-9} and optical spectrum after 500 km. (b) BER curves and corresponding eye diagrams at channel 7 after transmission.

improve by a 2-dB penalty than the NRZ-DPSK signals. It results from the fact that the RZ-DPSK signal has a data-independent intensity profile and removes the pattern effects in the nonlinear fiber. Fig. 14(c) presents the power penalties for all channels and compares them with back-to-back results at a BER of 10^{-9}. The inset figure within Fig. 14(c) is the received optical spectrum after the RZ-DPSK signal bidirectional transmission over 230 km for even channels. Due to the imperfect circulator and RB, the reflected even channels can be seen in this spectrum. This figure clearly indicates that the power penalties for all channels are less than 1.1 dB, and the differential between the bidirectional and unidirectional transmissions are less than 0.2 dB. These power penalties are attributed to residual dispersion and ASE accumulation due to SNR degradation.

To compare the performance of different inline amplifiers in this bidirectional configuration, we employed an SOA to supersede the dual-stage EDFA. To contrast with [13], only one common SOA has been exercised to realize bidirectional transmission. Due to the gain limitation of the SOA, we used an 80-km SSMF and the matching DCF in the transmission system. The SOA has a saturated power of 11 dBm, and it provides a gain of 14.3 dB to each wavelength channel. For comparison, an intensity modulator had replaced the PM in our system to generate OOK-modulated signals. DPSK demodulator was removed at the receiver, and all other conditions were maintained. The measured BER curves and typical eye diagrams of channel 4 with RZ-DPSK, NRZ-DPSK, and OOK modulation formats are depicted in Fig. 15. The power penalties of RZ-DPSK and OOK signals were about 0.2 and 1.6 dB, respectively. In this figure, the eye diagram of OOK signals was distorted. It probably resulted from the pattern-dependent effect caused by the gain saturation and the crosstalk induced by XGM between WDM channels in the SOA. Our experimental results show that it is advantageous to use RZ-DPSK with a dual-stage EDFA in fiber-optic transmission. However, DPSK is more immune to SOA-induced crosstalk than OOK.

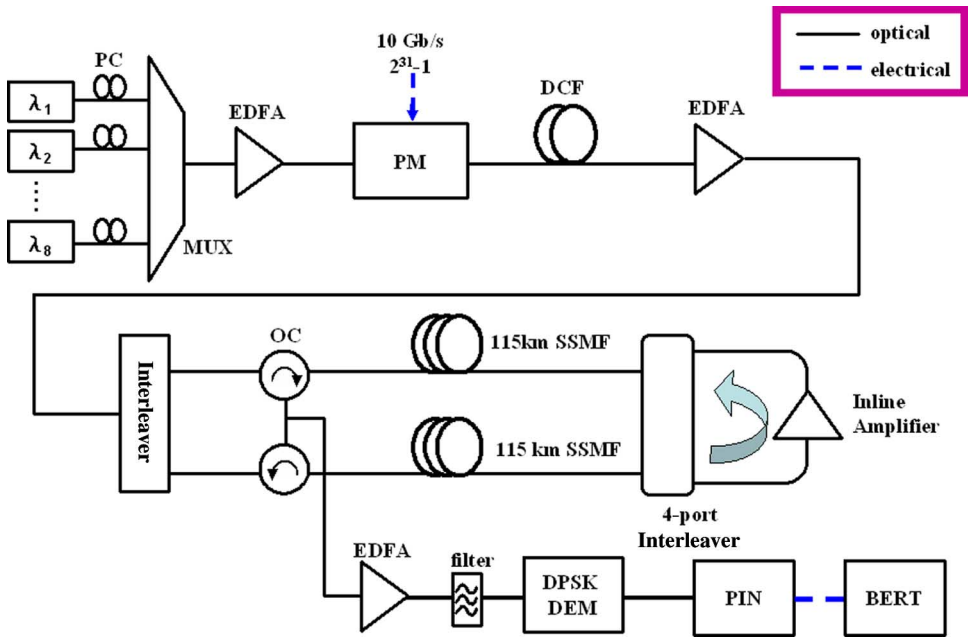

Fig. 13. Bidirectional DPSK transmission experimental setup.

Bidirectional RZ-DPSK transmission can be very beneficial in metro and access networks employing EDFAs as inline amplifiers.

V. Conclusion

We have successfully demonstrated novel three-port and four-port dispersion-free interleavers with temperature-compensated flat-top passband for bidirectional DWDM transmission systems. A three-port interleaver was modified to demonstrate a novel four-port interleaver with a 50-GHz channel spacing that enables bidirectional transmission using unidirectional amplification. Due to the complementary and wavelength-sensitive routing scheme, a dual-stage EDFA was employed to provide gain for bidirectional link. We had experimentally demonstrated this novel amplification scheme in strain line and recirculating loop transmission over 210 and 500 km with sensitivity penalties of less than 0.8 and 2.5 dB, respectively. For comparison, we also bitransmitted 10-Gb/s DPSK signals over 230 km. In this bidirectional configuration, RZ-DPSK signals, with an 1.1-dB sensitivity penalty, improved by a 2-dB penalty than NRZ-DPSK signals. The experimental results clearly demonstrate the feasibility of the bidirectional transmission utilizing the novel four-port interleaver. Furthermore, it is advantageous to use RZ-DPSK with dual-stage EDFA over SOA and other modulation formats in fiber-optic transmission. We believe that the design and configuration of our device can be scaled to more optical channels to 16 or 32 channels within the C-band. In analyzing the device performance, we also validated that the proposed interleaver design is capable of achieving DWDM spectral-efficient and crosstalk-tolerant signal transport for high-capacity bidirectional transmission systems.

Appendix

To estimate the influence of the dispersion of refractive index on an interleaver design, the dispersion must be included in the simulation model. From

$$[\Delta n_1(f_0)L_1 - \Delta n_2(f_0)L_2] = m\frac{c}{f_0} \tag{A1}$$

where $\Delta n_1(f_0) \equiv \Delta n_{10}$ and $\Delta n_2(f_0) \equiv \Delta n_{20}$ are the differences in the refractive index between the slow and fast axes of the birefringent crystals, respectively, m denotes the order of the wave plate, c represents the speed of light, and f_0 represents the center frequency, we arrive at

$$\frac{(\Delta n_{10}L_1 - \Delta n_{20}L_2)f_0}{c} = m \tag{A2}$$

$$\frac{[\Delta n_1(f_1)L_1 - \Delta n_2(f_1)L_2]\,f_1}{c} = m+1. \tag{A3}$$

Subtracting (A2) from (A3) yields

$$\frac{1}{c}\left[L_1\left(f_1\Delta n_1(f_1) - \Delta n_{10}f_0\right) - L_2\left(f_1\Delta n_2(f_1) - \Delta n_{210}f_0\right)\right] = 1. \tag{A4}$$

Using Taylor expansion of $\Delta n(f_1)$ around the center frequency f_0

$$\frac{1}{c}\left\{\left[L_1 f_1\left(\Delta n_{10} + \frac{d\Delta n_{10}}{df}(f_1 - f_0)\right) - \Delta n_{10}f_0\right] - \left[L_2 f_1\left(\Delta n_{20} + \frac{d\Delta n_{20}}{df}(f_1 - f_0)\right) - \Delta n_{20}f_0\right]\right\} \cong 1. \tag{A5}$$

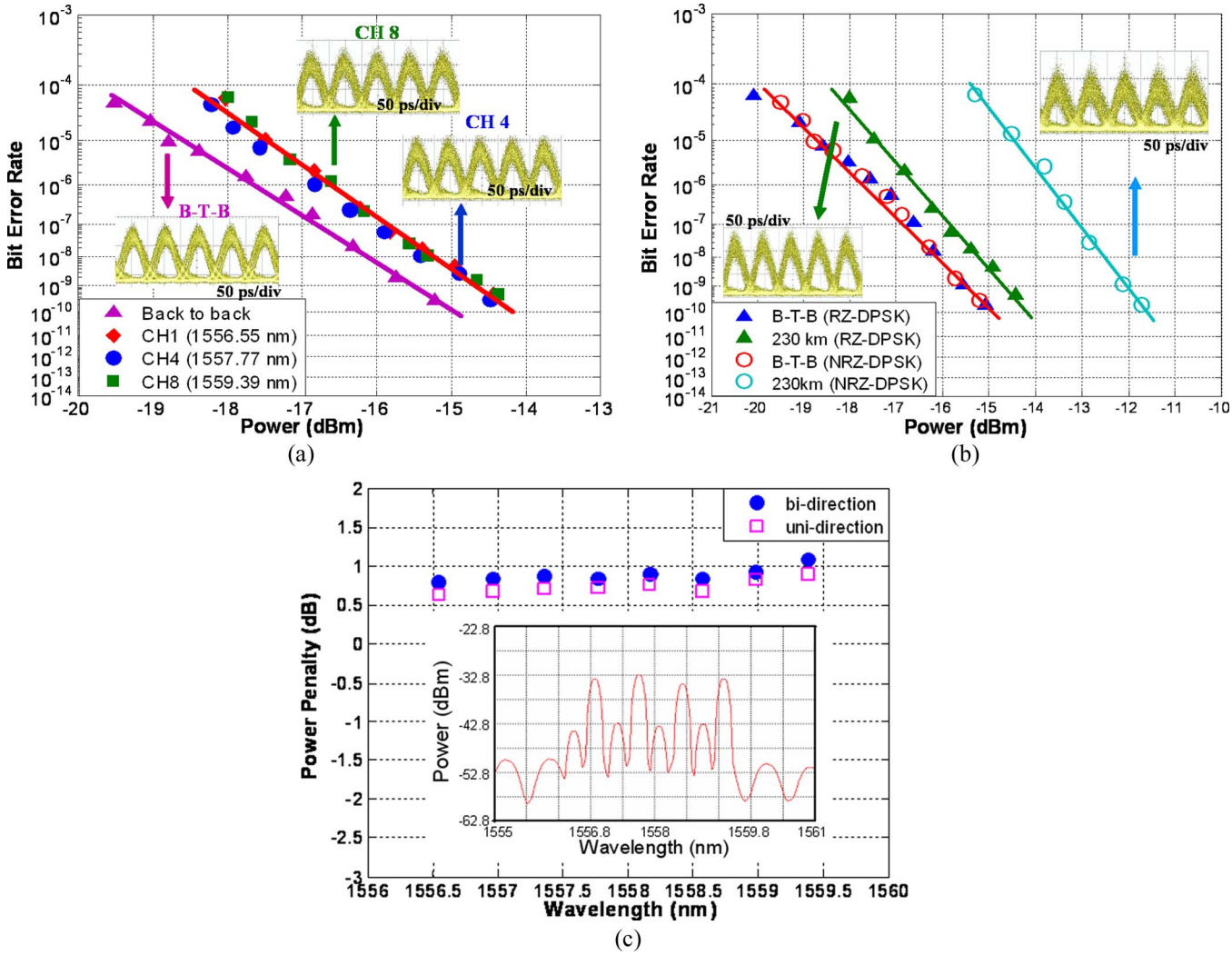

Fig. 14. (a) BER curves and corresponding eye diagrams of RZ-DPSK at channels 1, 4, and 8. (b) Comparison of RZ-DPSK and NRZ-DPSK at channel 4. (c) Received power penalties of all channels for the bidirectional and unidirectional transmissions at a BER of 10^{-9} and output optical spectrum of the bidirectional RZ-DPSK transmission after 230 km for even channels.

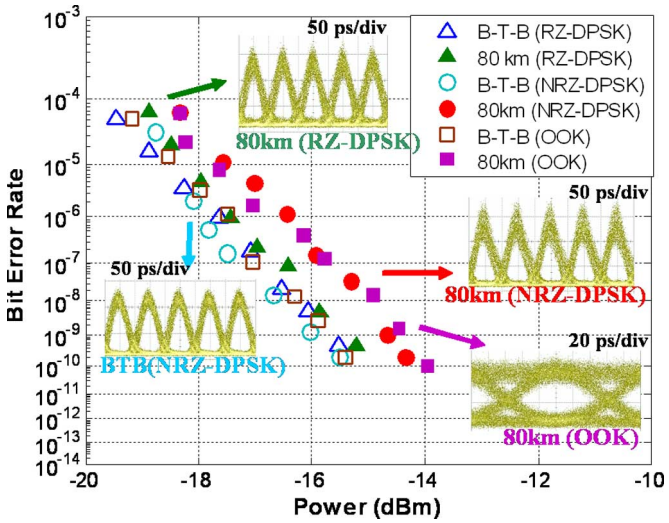

Fig. 15. BER curves and corresponding eye diagrams after 80 km of transmission by using a SOA as the inline amplifier.

Defining FSR $\equiv f_1 - f_0$, (A5) can be written as

$$\frac{\text{FSR}}{c}\left\{L_1\left[\Delta n_{10}+\frac{d\Delta n_1}{df_1}f_1\right] - L_2\left[\Delta n_{20}+\frac{d\Delta n_2}{df_2}f_2\right]\right\}\cong 1. \quad \text{(A6)}$$

With the group indexes Δn_{g10} and Δn_{g20}

$$\Delta n_{g0i}=\Delta n_{i0}+\frac{d\Delta n_{i0}}{df_i}f_i, \qquad i=1,2 \quad \text{(A7)}$$

$$\text{FSR}=\frac{c}{[L_1\Delta n_{g10}-L_2\Delta n_{g20}]}. \quad \text{(A8)}$$

The crystal length can then be selected using group indexes for eliminating the first-order error. For a typical C-band application, the frequency range of interest is around 4 THz (i.e., from 191.5 to 195.5 THz), with the center frequency at 193.5 THz. The frequency range corresponds to about 2% of the

center frequency. Owing to the small frequency range, the first-order approximation is justified and should provide a sufficient accuracy.

For a typical Mach–Zehnder interferometer, the transfer function can be written as

$$T(f) = \sin^2\left[\frac{k_{\text{eff}} L_{\text{eff}}}{2}\right] \cong \sin^2\left\{\frac{\pi}{c} f\left[L_1\left(\Delta n_{10} + \frac{d\Delta n_{10}}{df}(f - f_0)\right) - L_2\left(\Delta n_{20} + \frac{d\Delta n_{20}}{df}(f - f_0)\right)\right]\right\}. \quad \text{(A9)}$$

Inserting (A2) into (A9) yields

$$T(f) = \sin^2\left\{\frac{\pi}{c} f\left[L_1\left(\Delta n_{10} + \frac{d\Delta n_{10}}{df}(f - f_0)\right) - L_2\left(\Delta n_{20} + \frac{d\Delta n_{20}}{df}(f - f_0)\right)\right] - m\pi\right\} = \sin^2\left\{\frac{\pi}{c}\left[L_1\left[\Delta n_{10}(f - f_0) + \frac{d\Delta n_{10}}{df} f(f - f_0)\right] - L_2\left[\Delta n_{20}(f - f_0) + \frac{d\Delta n_{20}}{df} f(f - f_0)\right]\right]\right\}. \quad \text{(A10)}$$

After some calculations, we have

$$= \sin^2\left\{\frac{\pi}{\text{FSR}}(f - f_0) + \frac{\pi}{\text{FSR}} \frac{(f - f_0)^2}{L_1 \Delta n_{g10} - L_2 \Delta n_{g20}} \times \left[L_1 \frac{d\Delta n_{10}}{df} - L_2 \frac{d\Delta n_{20}}{df}\right]\right\}. \quad \text{(A11)}$$

The following observations can be drawn based on (A11).

1) A minimum occurs approximately every $(f - f_0) = k \cdot \text{FSR}$, and it is used as a basis for defining the FSR to the first order.
2) There is no first-order deviation if the group index n_g is selected, i.e., the error term $error \propto (f - f_0)$ disappeared.
3) The obtained offset is the second-order term, i.e.,

$$\frac{(f - f_0)^2}{L_1 n_{g10} - L_2 n_{g20}} \left[L_1 \frac{d\Delta n_{10}}{df} - L_2 \frac{d\Delta n_{20}}{df}\right].$$

The Sellmeier equation of YVO_4 and rutile can be used to calculate the slope of refractive indexes. Moreover, the typical values of the slope of the group index of YVO_4 and rutile are calculated as 1.05×10^{-4} and 1.72×10^{-4}, respectively. Table I lists some key parameters for 100-GHz interleavers. Table I can be used to estimate the deviation of FSR at the edge of frequency band. Fig. 16(a) shows the simulation and measurement results of the center wavelength offset and reveals the agreement between the measured results and the simulated prediction. For a C-band application with a total bandwidth of 4 THz, the frequency offset at 2 THz off the center is about 2.5 GHz. Fig. 16(b) shows the simulated results of the center frequency offset with different selected center frequencies. Because the frequency offset hyperbolically increases with the frequency range, the effective bandwidth decreases faster at the band edge. The center frequency offset caused by the refractive index dispersion is one inherited design issue due to the material refractive index dispersion. Therefore, different sets of crystal lengths are required for C-band and L-band applications to mitigate the center frequency offset.

TABLE I
SUMMARY OF THE KEY PARAMETERS FOR THE 100-GHz INTERLEAVER

Materials	Group Index Difference @ 193.5THz	Crystal Length (mm)	β (1/°C)	Slope of Group Index Difference (1/THz)
YVO_4	0.2139	9.5697	-26.54×10^{-6}	1.05×10^{-4}
Rutile	0.2652	2.0685	-99.06×10^{-6}	1.72×10^{-4}

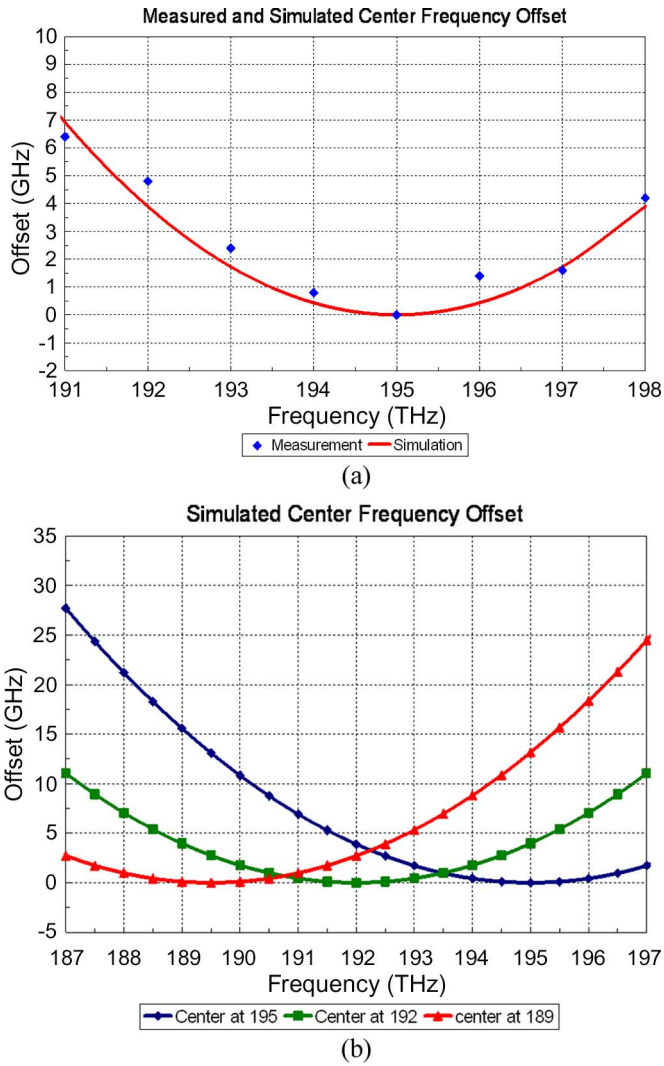

Fig. 16. (a) Measurement and simulation results of center frequency offset due to dispersion. (b) Center frequency offset with different selected center frequencies.

REFERENCES

[1] K. Jinguji and M. Oguma, "Optical half-band filters," *J. Lightw. Technol.*, vol. 18, no. 2, pp. 252–259, Feb. 2000.

[2] S. Cao, J. Chen, J. N. Damask, C. R. Doerr, L. Guiziou, G. Harvey, Y. Hibino, H. Li, S. Suzuki, K.-Y. Wu, and P. Xie, "Interleaver technology: Comparisons and applications requirements," *J. Lightw. Technol.*, vol. 22, no. 1, pp. 281–289, Jan. 2004.

[3] K. Tai, B. Chang, J. Chen, C. Mao, T. Ducellier, J. Xie, L. Mao, and J. Wheeldon, "Wavelength-interleaving bidirectional circulators," *IEEE Photon. Technol. Lett.*, vol. 13, no. 4, pp. 320–322, Apr. 2001.

[4] S. Y. Kim, S. H. Lee, S. S. Lee, and J. S. Lee, "Upgrading WDM networks using ultradense WDM channel groups," *IEEE Photon. Technol. Lett.*, vol. 16, no. 8, pp. 1966–1968, Aug. 2004.

[5] H. S. Chung, J. S. Han, S. H. Chang, and H. J. Lee, "Bidirectional transmissions of 32 channels × 10 Gb/s over metropolitan networks using xs," *IEEE Photon. Technol. Lett.*, vol. 16, no. 4, pp. 1194–1196, Apr. 2004.

[6] S. T. Lee and C. J. Chae, "Low-cost bidirectional optical amplifier using a single EDFA and a 4-port wavelength interleaver," in *Proc. 13th Annu. Meeting. IEEE LEOS*, 2000, vol. 1, pp. 277–278.

[7] M. F. Huang, J. Chen, K. M. Feng, C. C. Wei, C. Y. Lai, T. Y. Lin, and S. Chi, "210-km Bidirectional transmission system with a novel four-port interleaver to facilitate unidirectional amplification," *IEEE Photon. Technol. Lett.*, vol. 18, no. 1, pp. 172–174, Jan. 2006.

[8] S. Radic, S. Chandrasekhar, A. Srivastava, H. Kim, L. Nelson, S. Liang, K. Tai, and N. Copner, "Dense interleaved bidirectional transmission over 5 × 80 km of nonzero dispersion-shifted fiber," *IEEE Photon. Technol. Lett.*, vol. 14, no. 2, pp. 218–220, Feb. 2002.

[9] M. D. Feuer, "Measurement of OSNR in the presence of partially polarized ASE," *IEEE Photon. Technol. Lett.*, vol. 17, no. 2, pp. 435–437, Feb. 2005.

[10] J. Yu, A. Buxens, A. Clausen, and P. Jeppesen, "16 × 10 Gb/s WDM bidirectional gating in a semiconductor optical amplifier for optical cross connects exploiting network connection symmetry," *IEEE Photon. Technol. Lett.*, vol. 12, no. 6, pp. 702–704, Jun. 2000.

[11] A. H. Gnauck, G. Raybon, S. Chandrasekhar, J. Leuthold, C. Doerr, L. Stulz, A. Agarwal, S. Banerjee, D. Grosz, S. Hunsche, A. Kung, A. Marhelyuk, D. Maywar, M. Movassaghi, X. Liu, C. Xu, X. Wei, and D. M. Gill, "2.5 Tb/s (64 × 42.7 Gb/s) transmission over 40 × 100 km NZDSF using RZ-DPSK format and all-Raman-amplified spans," in *Proc. OFC*, Anaheim, CA, 2002, pp. FC2-1–FC2-3.

[12] J. Yu, Y. K. Yeo, O. Akanbi, and G. K. Chang, "Bi-directional transmission of 8 × 10 Gb/s DPSK signals over 80 km of SMF-28 fiber using in-line semiconductor optical amplifier," *Opt. Express*, vol. 12, no. 25, pp. 6215–6218, Dec. 2004.

[13] R. Proietti, A. D'Errico, L. Giorgi, N. Calabretta, G. Contestabile, and E. Ciaramella, "16 × 10 Gb/s DPSK transmission over 140-km SSMF by using two common SOAs," *IEEE Photon. Technol. Lett.*, vol. 18, no. 15, pp. 1675–1677, Aug. 2006.

[14] V. S. Grigoryan, M. Shin, P. Devgan, J. Lasri, and P. Kumar, "SOA-based regenerative amplification of phase-noise-degraded DPSK signals: Dynamic analysis and demonstration," *J. Lightw. Technol.*, vol. 24, no. 1, pp. 135–142, Jan. 2006.

[15] T. Mizuochi, K. Ishida, T. Kobayashi, J. Abe, K. Kinjo, K. Motoshima, and K. Kasahara, "A comparative study of DPSK and OOK WDM transmission over transoceanic distances and their performance degradations due to nonlinear phase noise," *J. Lightw. Technol.*, vol. 21, no. 9, pp. 1933–1943, Sep. 2003.

[16] B. Lyot, "Optical apparatus with wide field using interference of polarized light," *C. R. Acad. Sci. (Paris)*, vol. 195, pp. 1593–1597, 1993.

[17] Y. Öhman, "A new monochromator," *Nature*, vol. 41, pp. 291–296, 1938.

[18] I. Šolc, "Birefringent chain filters," *J. Opt. Soc. Amer.*, vol. 55, no. 6, pp. 621–624, 1965.

[19] J. Chen, "Dispersion-compensating optical digital filters for 40-Gb/s metro add–drop applications," *IEEE Photon. Technol. Lett.*, vol. 16, no. 5, pp. 1310–1312, May 2004.

[20] M. F. Huang, K. M. Feng, J. Chen, T. Y. Lin, C. C. Wei, and S. Chi, "Wavelength-interleaving bidirectional transmission system using unidirectional amplification in a 5 × 100 km recirculating loop," *IEEE Photon. Technol. Lett.*, vol. 18, no. 12, pp. 1326–1328, Jun. 2006.

[21] K. M. Feng, M. F. Huang, C. C. Wei, C. Y. Lai, T. Y. Lin, J. Chen, and S. Chi, "Metro add–drop network applications of cascaded dispersion-compensated interleaver pairs using a recirculating loop," *IEEE Photon. Technol. Lett.*, vol. 17, no. 6, pp. 1349–1351, Jun. 2005.

Ming-Fang Huang (S'04) received the B.S. degree in physics from Tamkang University, Taipei, Taiwan, R.O.C., in 2001 and the M.S. degree in electrooptical engineering from the National Chiao Tung University, Hsinchu, Taiwan, in 2003. She is currently working toward the Ph.D. degree in electrooptical engineering at the National Chiao Tung University.

She is a Researcher with the School of Electrical and Computer Engineering, Georgia Institute of Technology, Atlanta. Her current research interests include long-haul transmission, new modulation format technologies, wavelength-division multiplexing passive optical networks (PONs), and time-division multiplexing PONs.

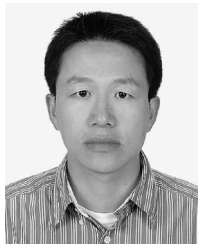

Jason (Jyehong) Chen (M'00) received the B.S. and M.S. degrees in electrical engineering from the National Taiwan University, Taipei, Taiwan, R.O.C., in 1988 and 1990, respectively, and the Ph.D. degree in electrical engineering and computer science from the University of Maryland Baltimore County, Baltimore, in 1998.

In 1998, he joined JDS Uniphase as a Senior Engineer. In 2003, he joined the faculty of the National Chiao Tung University, Hsinchu, Taiwan, where he is currently an Associate Professor with the Institute of Electro-Optical Engineering and Department of Photonics. He is the holder of ten U.S. patents.

Jianjun Yu (M'03–SM'04) received the B.S. degree in optics from Xiangtan University, Xiangtan, China, in 1990 and the M.E. and Ph.D. degrees in optical communications from the Beijing University of Posts and Telecommunications, Beijing, China, in 1996 and 1999, respectively.

From June 1999 to January 2001, he was an Assistant Research Professor with the Research Center for Communications, Optics, and Materials, Technical University of Denmark, Lyngby, Denmark. From February 2001 to December 2002, he was a member of Technical Staff with Lucent Technologies and Agere Systems, Murray Hill, NJ. In January 2003, he joined the Georgia Institute of Technology, Atlanta, where he was a Research Faculty and served as the Director of the Optical Network Laboratory. He is currently a Member of Technical Staff with NEC Laboratories America, Princeton, NJ. He is also an Adjunct Professor with the Georgia Institute of Technology and the Beijing University of Posts and Telecommunications. As the first author, he has more than 100 papers published in international journals and conference proceedings. He is the holder of two U.S. patents with five others pending. He serves as a reviewer for *Optics Letters*, *Electronics Letters*, *Optics Express*, *Optical Engineering*, and *Optics Communications*. His current research interests include new modulation format techniques, radio-over-fiber systems and networks, wavelength-division multiplexing passive optical networks, and optical label switching in optical networks.

Dr. Yu is a Senior member of the IEEE Lasers and Electro-Optics Society (LEOS). He served as a Guest Editor of the Special Issue on Convergence of Optical and Wireless Networks of the IEEE/OSA JOURNAL OF LIGHTWAVE TECHNOLOGY. He serves as a Technical Committee member of the IEEE LEOS 2005–2007 Annual Meeting, as well as a reviewer for the IEEE PHOTONICS TECHNOLOGY LETTERS, JOURNAL OF LIGHTWAVE TECHNOLOGY, and IEEE JOURNAL OF QUANTUM ELECTRONICS.

Sien Chi received the B.S.E.E. degree from the National Taiwan University, Taipei, Taiwan, R.O.C., in 1959, the M.S.E.E. degree from the National Chiao Tung University, Hsinchu, Taiwan, in 1961, and the Ph.D. degree in electrophysics from the Polytechnic Institute, Brooklyn, NY, in 1971.

From 1971 to 2004, he was a Professor with the National Chiao Tung University. From 1998 to 2001, he was the Vice President of the National Chiao Tung University. He is currently a Chair Professor with Yuan Ze University, Chungli, Taiwan. His research interests include optical fiber communications, optical solitons, optical modulation format, and optical fiber amplifiers.

Prof. Chi is a Fellow of the Optical Society of America.

Gee-Kung Chang (M'80–SM'92–F'05) received the B.S. degree in physics from the National Tsinghua University, Hsinchu, Taiwan, R.O.C., and the M.S. and Ph.D. degrees in physics from the University of California, Riverside.

He is the Byers Endowed Chair Professor of Optical Networking with the School of Electrical and Computer Engineering, Georgia Institute of Technology (Georgia Tech), Atlanta, and an Eminent Scholar of the Georgia Research Alliance. He serves as the Leader and Associate Director of the Optoelectronics Integration and Packaging Alliance of the National Science Foundation-funded Engineering Research Center Microsystem Packaging Research Center, Georgia Tech. He is also an Associate Director of the Georgia Tech Broadband Institute. He devoted a total of 23 years of service to the Bell Systems—Bell Laboratories, Bellcore, and Telcordia Technologies—where he served in various research and management positions, including Director and Chief Scientist of Optical Internet Research, Director of the Optical Networking Systems and Testbed, and Director of the Optical System Integration and Network Interoperability. Prior to joining Georgia Tech, he served as Vice President and Chief Technology Strategist with OpNext, Inc., a spin-out of Hitachi Telecom, where he was in charge of technology planning and product strategy for advanced high-speed optoelectronic components and systems for computing and communication systems. He has coauthored more than 230 papers published in peer-reviewed journals and conference proceedings. He is the holder of 40 U.S. patents in the area of optoelectronic devices, high-speed integrated circuits, optoelectronics switching components for computing and communication systems, WDM optical networking elements and systems, multiwavelength optical networks, optical network security, optical label switching routers, and optical interconnects for next-generation servers and computers.

Dr. Chang is a Fellow of the IEEE Lasers and Electro-Optics Society (LEOS) and the Optical Society of America (OSA) for his contributions to DWDM optical networking and label switching technologies. He was elected as a Telcordia Fellow in 1999 for pioneering work in the optical networking projects MONET and NGI. He became a Fellow of the Photonic Society of Chinese–Americans in 2000. He has been serving on many IEEE LEOS and OSA conferences and committees. He has served three times as the Lead Guest Editor for special issues of the JOURNAL OF LIGHTWAVE TECHNOLOGY sponsored by IEEE LEOS and OSA. The first issue was published in December 2000 on Optical Networks, the second one in November 2004 on Metro and Access Networks, and an upcoming one in 2007 on the Convergence of Optical Wireless Access Networks. He was the recipient of the Bellcore President's Award in 1994 for his leadership role in the Optical Networking Technology Consortium and the R&D 100 Award in 1996 for his contribution to network access modules.